



ARTICLE

Received 15 Jan 2014 | Accepted 4 Jun 2014 | Published 7 Jul 2014

DOI: 10.1038/ncomms5291

Suppression of the critical thickness threshold for conductivity at the LaAlO₃/SrTiO₃ interface

E. Lesne¹, N. Reyren¹, D. Doennig², R. Mattana¹, H. Jaffrès¹, V. Cros¹, F. Petroff¹, F. Choueikani³, P. Ohresser³, R. Pentcheva^{2,4}, A. Barthélémy¹ & M. Bibes¹

Perovskite materials engineered in epitaxial heterostructures have been intensely investigated during the last decade. The interface formed by an LaAlO₃ thin film grown on top of a TiO₂-terminated SrTiO₃ substrate hosts a two-dimensional electronic system and has become the prototypical example of this field. Although controversy exists regarding some of its physical properties and their precise origin, it is universally found that conductivity only appears beyond an LaAlO₃ thickness threshold of four unit cells. Here, we experimentally demonstrate that this critical thickness can be reduced to just one unit cell when a metallic film of cobalt is deposited on top of LaAlO₃. First-principles calculations indicate that Co modifies the electrostatic boundary conditions and induces a charge transfer towards the Ti 3d bands, supporting the electrostatic origin of the electronic system at the LaAlO₃/SrTiO₃ interface. Our results expand the interest of this low-dimensional oxide system from in-plane to perpendicular transport and to the exploration of elastic and inelastic tunnel-type transport of (spin-polarized) carriers.

¹Unité Mixte de Physique CNRS/Thales, 1 Avenue A. Fresnel, 91767 Palaiseau, France and Université Paris-Sud, 91405 Orsay, France. ²Department of Earth and Environmental Sciences, Section Crystallography and Center of Nanoscience (CENS), University of Munich, Theresienstrasse 41, DE-80333 Munich, Germany. ³Synchrotron SOLEIL, L'Orme des Merisiers, Saint-Aubin, BP 48, 91192 Gif-sur-Yvette, France. ⁴Faculty of Physics, University of Duisburg-Essen, D-47048 Duisburg, Germany. Correspondence and requests for materials should be addressed to E.L. (email: edouard.lesne@thalesgroup.com) or to M.B. (email: manuel.bibes@thalesgroup.com).

Combined in heterostructures, oxide thin films offer a new playground with virtually unlimited combinations to realize artificial systems and to explore emerging phenomena absent in bulk compounds¹. Ohtomo and Hwang² striking discovery of conducting LaAlO₃/SrTiO₃ heterointerfaces has fast-tracked this system as the fruit fly for such investigations. The LaAlO₃/SrTiO₃ system exhibits gate-tunable quasi-two-dimensional electronic conduction³, Rashba spin-orbit interaction^{4,5} and superconductivity^{6–8}, displays indications of magnetism^{9,10} and even close coexistence of the latter two^{11–13}. This makes the LaAlO₃/SrTiO₃ system attractive for fundamental studies as well as promising for potential applications such as oxide-based electronics^{14–16}.

While the perovskite crystals LaAlO₃ (LAO) and SrTiO₃ (STO) are both wide band-gap insulators, the growth of an epitaxial LAO film on a TiO₂-terminated, (001)-oriented STO substrate leads to an insulator-to-metal transition when the LAO thickness reaches 4 unit cells (uc)³. Owing to their ionic nature, the STO(001) substrate (non-polar) and the LAO(001) film (polar) form a strongly polar interface. This results in an electrostatic potential that increases as the LAO thickness is increased, leading to an electronic reconstruction with charge transferred towards the STO top-TiO₂ subplane¹⁷.

Recently, first-principles calculations predicted a conductive system at the LAO/STO interface for heterostructures with various metallic capping layers, and an LAO thickness of 2 uc¹⁸. In this letter, we present results of electrical magnetotransport and X-ray absorption spectroscopy (XAS) experiments on LAO/STO samples with either bare LAO surfaces or a metallic capping layer of cobalt, combined with density functional theory (DFT) calculations. We demonstrate the existence of metallic conductivity on the STO side for an LAO thickness as thin as 1 uc.

Results

Magnetotransport measurements of Co/LAO/STO samples.

LAO films were grown by pulsed laser deposition (PLD) on TiO₂-terminated STO(001) substrates and followed by *in situ* magnetron sputtering deposition of a 2–2.5-nm cobalt thin film, capped with a 3-nm AlO_x layer to prevent Co oxidation. Details

concerning samples fabrication and characterization can be found in the Methods section and in the Supplementary Information (Supplementary Note 1).

The unpatterned samples were electrically contacted with aluminium wires by ultrasonic wedge bonding. Four-point transport measurements (in-plane longitudinal R_{xx} and transverse R_{xy} magnetoresistances) were performed by connecting the corners of the square sample in the van der Pauw geometry. Figure 1a shows the measured in-plane longitudinal resistance R_{xx}^{meas} versus temperature of Co/LAO/STO heterostructures with various LAO thicknesses, and of a Co/STO control sample for which the STO substrate experienced the same procedure of thermal and oxygen pressure cycles as for the LAO/STO samples. While the Co/STO sample shows very little variation of its resistance (<1%) across the explored temperature range, the Co-capped LAO/STO samples display a strong reduction in their resistance as temperature is decreased, which readily suggests that the LAO/STO interface conducts, even for samples with an LAO film thickness smaller than 4 uc.

Following these observations, we now model the Co/LAO($n \geq 1$ uc)/STO heterostructures by two conducting layers in parallel composed of the Co overlayer and the STO sublayer. According to this simple picture, and supposing a temperature-independent resistance of the Co capping layer (see Fig. 1a; Supplementary Fig. 1), the temperature evolution of the STO sublayer's longitudinal resistance is given by:

$$R_{xx}^{\text{STO}}(T) = \frac{R_{xx}^{\text{Co}} \cdot R_{xx}^{\text{meas}}(T)}{R_{xx}^{\text{Co}} - R_{xx}^{\text{meas}}(T)}. \quad (1)$$

The sheet resistance of the STO sublayer is defined as $R_{\square}^{\text{STO}} = R_{xx}^{\text{STO}}(T) \times \frac{\pi}{\ln(2)}$, assuming a homogeneous conductance in the geometry of the inset of Fig. 1a¹⁹, supported by the fact that $R_{xx} \approx R_{yy}$ within a few percent. For each sample, we calculate $R_{xx}^{\text{STO}}(T)$ by taking the data set as $R_{xx}^{\text{meas}}(T)$, and R_{xx}^{Co} as the measured value at room temperature ($R_{xx}^{\text{Co}} = R_{xx}^{\text{meas}}(290\text{K})$) for the corresponding sample. Figure 1b displays the calculated sheet resistance R_{\square}^{STO} of the Co/LAO/STO samples in the low-temperature range (below 100 K).

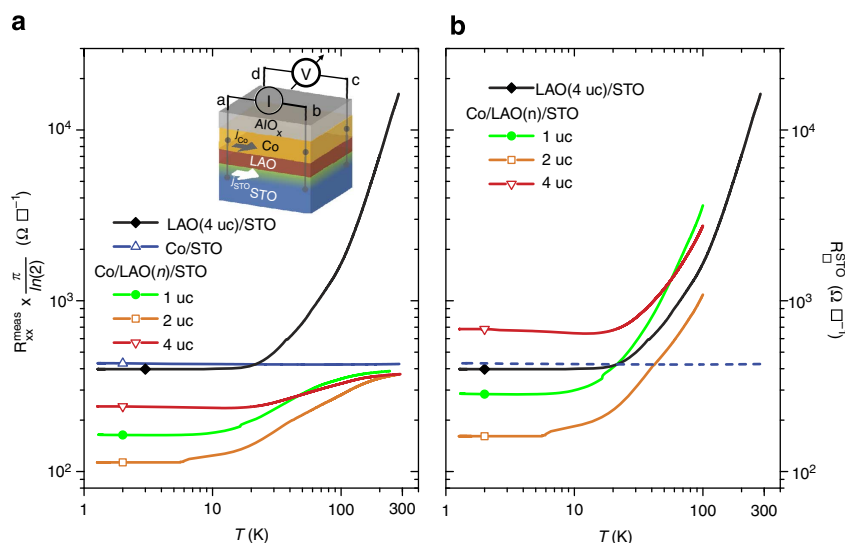


Figure 1 | Sheet resistances as a function of temperature. (a) Measured longitudinal resistance R_{xx}^{meas} versus temperature T of LAO(4 uc)/STO and Co/LAO(n)/STO samples showing a clear metallic behaviour. The Co/STO resistance remains almost unchanged from 300 to 1.4 K ($\Delta R/R < 1\%$). Inset: measurement configuration. The thick arrows in the sketch represent the current flowing in the Co layer and in the STO. (b) Calculated sheet resistance R_{\square}^{STO} of the conducting STO sublayer in Co/LAO(n)/STO samples (according to equation (1)), and measured sheet resistance of the LAO(4 uc)/STO samples. The blue dotted line corresponds to the Co/STO data set.

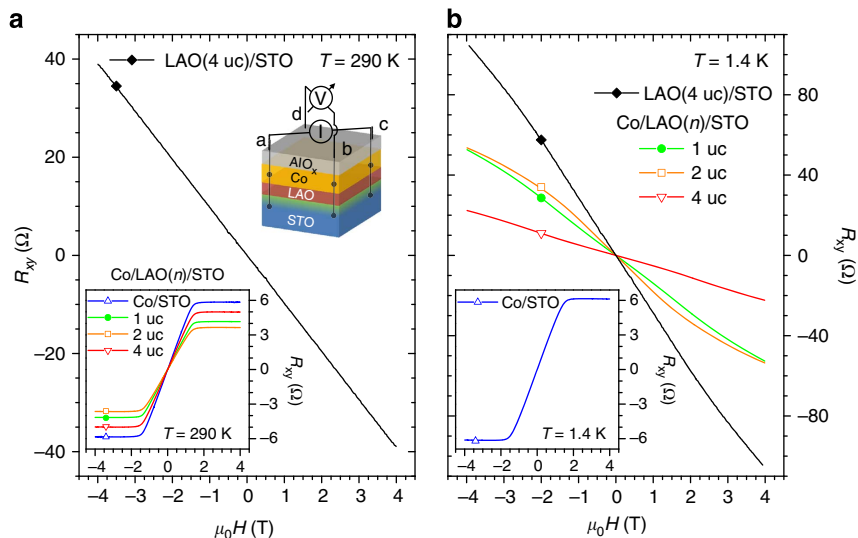


Figure 2 | Hall effect measurements. (a) Antisymmetrized Hall resistance R_{xy} as a function of applied magnetic field μ_0H of an LAO(4 uc)/STO sample displaying a linear Hall effect at room temperature. Inset: R_{xy} versus μ_0H for various Co/LAO(n)/STO samples at 290 K showing cobalt dominated AHE at low magnetic field. (b) Antisymmetrized Hall resistance R_{xy} versus μ_0H of an LAO(4 uc)/STO sample and of Co/LAO(n)/STO at 1.4 K. Inset: R_{xy} versus μ_0H for Co/STO at 1.4 K similar to the one observed at 290 K.

Next, we focus on transport experiments carried out in Hall configuration at room temperature and at low temperature (1.4 K). The measured transverse magnetoresistance curves were antisymmetrized ($R_{xy}(H) = [R_{xy}^{\text{meas}}(H) - R_{xy}^{\text{meas}}(-H)]/2$). Antisymmetrized traces $R_{ac-db}(H)$ and $R_{db-ca}(H)$ appear indistinguishable in Fig. 2a,b, suggesting again good sample homogeneity and no artefacts due to the data analysis. In the case of the LAO(4 uc)/STO sample, Hall measurements taken at room temperature show a linear behaviour for magnetic field up to 4 T (see Fig. 2a) with an extracted sheet carrier density $n_{\square} = 6.4 \times 10^{13} \text{ cm}^{-2}$. In contrast, Co/STO and Co/LAO/STO samples exhibit at room temperature a Hall effect dominated by the cobalt layer, independent of the LAO thickness (see inset of Fig. 2a), with a low-magnetic-field regime ($|\mu_0H| \leq 1.2$ T) displaying the anomalous Hall effect characteristic of a ferromagnetic metal. In the high-field regime ($|\mu_0H| \geq 2.2$ T), the Co magnetization is rotated out of plane and the Co-capped samples exhibit a normal Hall effect with a weak negative slope of order $-10 \text{ m}\Omega \text{ T}^{-1}$ (that is a carrier density of order 10^{23} cm^{-3}).

Figure 2b displays Hall data acquired at 1.4 K. $R_{xy}(H)$ measured at 1.4 K in Co/STO shows essentially no change when compared with room temperature measurements (see insets of Fig. 2a,b). On the other hand, $R_{xy}(H)$ behaviour of Co/LAO($n = 1, 2, 4$ uc)/STO samples at 1.4 K display striking similarities with those carried out on uncapped LAO(4 uc)/STO samples. The Hall resistance trace of the LAO(4 uc)/STO sample is not purely linear at 1.4 K, a behaviour believed to arise from the multi-band structure of STO^{20–22}. Evidence for this is given from the DFT calculations in the Supplementary Information (see Supplementary Fig. 2). We only consider the ‘high field’ regime ($|\mu_0H| \geq 3$ T) where n_{\square} , the total electron density in the STO, is given by $n_{\square} = -\frac{1}{|e| \cdot R_H}$, with e the elementary charge and R_H the Hall coefficient determined for $|\mu_0H| \geq 3$ T. The kink observed in the LAO(4 uc)/STO Hall trace $R_{xy}(H)$ is well reproduced in Co-capped LAO samples at 1.4 K, regardless of the LAO thickness. This close resemblance for both sets of samples suggests a common host for the observed electronic transport. The measured Hall coefficients, and related carrier densities show no correlation with LAO thickness. Taking the sheet resistance and Hall coefficient at 1.4 K, one can estimate the electronic mobility $\mu_H^{\text{STO}} = R_H/R_{\square}^{\text{STO}}$ of the STO sublayer in Co/LAO/STO

samples. Values in the range of $(1 - 6 \times 10^2 \text{ cm}^2 \text{ V}^{-1} \text{ s}^{-1})$ are found. We note that the very thin Co layer is not expected to play a role in Hall effect measurements at 1.4 K, owing to its much lower mobility ($\mu_H^{\text{Co}} < 1 \text{ cm}^2 \text{ V}^{-1} \text{ s}^{-1}$ determined experimentally), thus supporting our simple analysis.

Hence, our transport data collected on Co/LAO/STO heterostructures clearly indicate the presence of an electronic system at the LAO/STO interface whose behaviour is very similar to the usual LAO($n \geq 4$ uc)/STO, even for LAO as thin as a single unit cell. Furthermore, the estimated carrier densities (several $10^{13} - 10^{14} \text{ cm}^{-2}$) in Co/LAO/STO samples are comparable to values typically found for quasi-two-dimensional electronic systems at LAO/STO interfaces^{3,23,24}.

X-ray absorption spectroscopy experiments. To gain further insight into the electronic structure of Co/LAO/STO systems, we have performed XAS measurements at the DEIMOS beamline of Synchrotron SOLEIL²⁵. XAS probes transition from core electronic states to excited electronic states. The energy of the incident X-ray beam can be tuned to the Ti $L_{2,3}$ absorption edge to probe electronic transitions from $2p_{3/2}$ and $2p_{1/2}$ to $3d$ levels (see Fig. 3a)²⁶. Therefore, the preferential occupancy of states with different orbital symmetries can be probed by X-ray linear dichroism (XLD), which is the difference in XAS measured with a linear horizontal (LH) or vertical (LV) polarization of the X-ray beam (see Fig. 3b), that is, $\text{XLD} = (\text{LH} - \text{LV})$. Conversely, the isotropic signal is defined as the mean of the two: $\text{ISO} = (\text{LH} + \text{LV})/2$.

The XAS experiments were performed at the Ti $L_{2,3}$ absorption edge, on the same Co/STO and Co/LAO(2 uc)/STO samples previously shown in Figs 1 and 2, as well as on a bare STO substrate, on an insulating LAO(2 uc)/STO heterostructure and on a conducting LAO(4 uc)/STO sample. All spectra were collected at 300 K in total electron yield mode in order to be surface sensitive. In Fig. 3, the ISO signals appear to be largely of Ti^{4+} character for all samples²⁷. The XLD signals, however, display significant differences between the samples (see Fig. 3d). In LAO/STO samples with 2 and 4 uc of LAO, the XLD shows a sign reversal with respect to that obtained from a bare STO substrate. This is related to an inverted (negative versus positive)

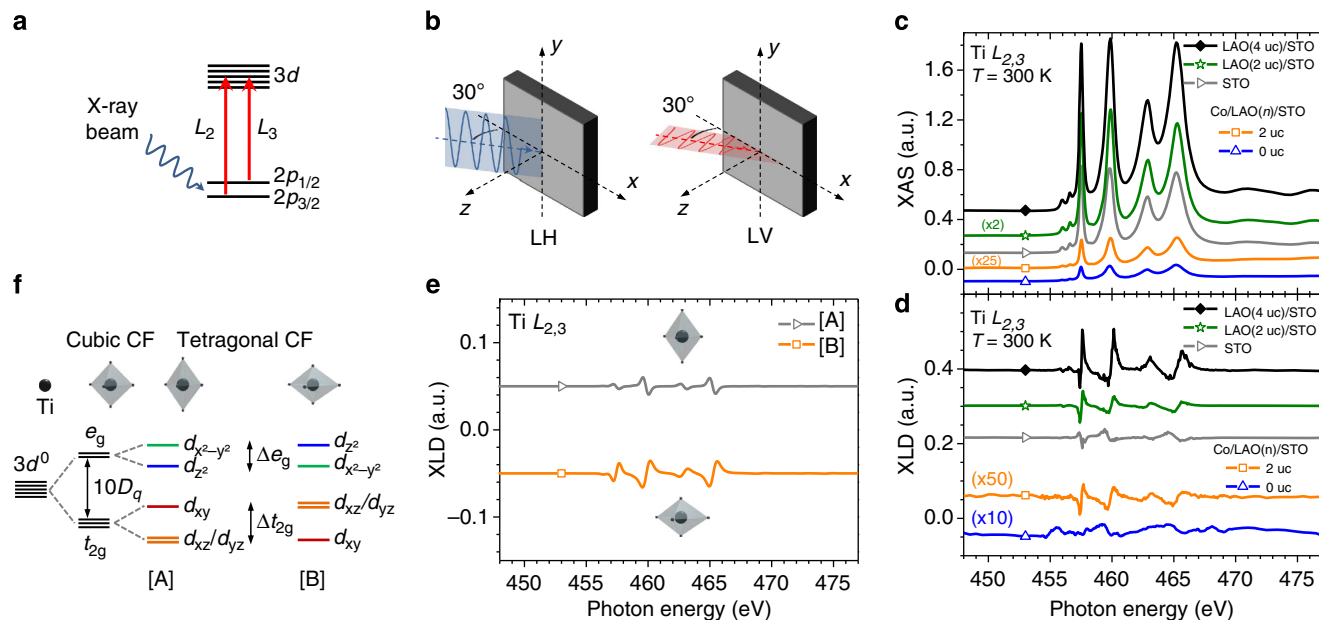


Figure 3 | X-ray absorption spectroscopy at Ti $L_{2,3}$ edge. (a) Sketch of the X-ray absorption spectroscopy (XAS) process depicting the $2p \rightarrow 3d$ electronic transitions at the Ti $L_{2,3}$ edge. (b) Scheme of the XAS measurement geometries with linearly horizontal (LH) and linearly vertical (LV) polarized light. The incident beam forms a 30° angle with the sample surface (x, y). (c) Experimentally measured isotropic signals (ISO) versus photon energy of a STO(001) substrate, and of various (Co)/LAO(n)/STO samples. Spectra acquired at 300 K in total electron yield mode. (d) The corresponding experimental X-ray linear dichroism (XLD) signals show a sign inversion between the XLD of STO and Co/STO and that of LAO(2,4 uc) and Co/LAO(2 uc) samples. (e) Calculated XLD that reproduces the experimental XLD of the STO bare substrate (circle, [A]) and of the Co/LAO(2 uc)/STO sample (square, [B]). (f) The cubic crystal field (CF) splits the Ti^{4+} $3d$ states into e_g and t_{2g} levels. A tetragonal CF further lifts the orbital degeneracy, with: [A] case of STO, [B] case of (Co)/LAO/STO.

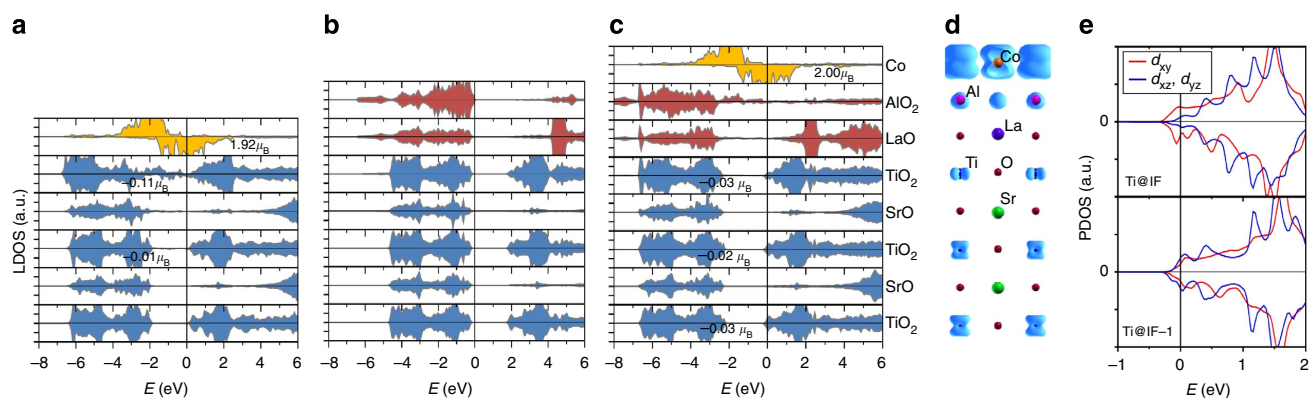


Figure 4 | Layer-resolved density of states. LDOS of (a) Co(1 ML)/STO, (b) LAO(1 uc)/STO and (c) Co(1 ML)/LAO(1 uc)/STO heterostructures within GGA with a 4.5-uc-thick STO substrate. (d) Side view of Co(1 ML)/LAO(1 uc)/STO with the electron density integrated in the interval $E_F - 0.50$ eV to E_F , giving insight into the Ti $3d$ orbital occupation, where $E = E_F = 0$ corresponds to the Fermi level. (e) Projected density of states (PDOS) of Ti in the interface (IF) and IF-1 layer of Co/LAO(1 uc)/STO. Positive (negative) values correspond to majority (minority) spin.

splitting of the $3d$ bands (see Fig. 3f). Interestingly, the XLD measured on the Co/LAO(2 uc)/STO sample is also very different from that of the STO substrate and appears very similar to the uncapped LAO/STO samples. Although much noisier, the XLD signal of the Co/STO sample resembles that of the bare STO.

In bulk cubic STO, the crystal field splits the fivefold degenerate Ti $3d$ bands into twofold e_g ($d_{x^2-y^2}$, d_{z^2}) and threefold t_{2g} (d_{xy} , d_{xz} , d_{yz}) degenerate bands²⁸. In an attempt to clarify this band picture, we have performed atomic multiplet calculations using the CTM4XAS program²⁹. It allowed us to explore the effect of a symmetry reduction of the system (for example, towards tetragonal), which distorts the TiO_6 octahedra and lifts the degeneracy of the e_g and t_{2g} bands (see Fig. 3e,f). The measured XLD were well reproduced by using

values of the energy splittings identical to those reported in the literature^{30,31}. In the case of STO, we considered positive energy splittings $\Delta e_g = 40$ meV and $\Delta t_{2g} = 25$ meV³⁰. In contrast, for the LAO/STO and Co/LAO/STO systems, negative energy splittings $\Delta e_g = -100$ meV and $\Delta t_{2g} = -50$ meV were considered³¹. We note that introducing a Co capping layer does not alter the fine structure of the XLD observed in uncapped LAO/STO samples. Interestingly, we have shown that Co-capped and uncapped LAO/STO systems have a similar subband structure, with a preferential d_{xy} orbital occupancy.

Incidentally, we performed X-ray magnetic circular dichroism experiments at the Ti $L_{2,3}$ edge on Co/LAO(n)/STO samples with $n = 2$ and 4 uc samples (see Supplementary Fig. 3). The signal-to-noise ratio of our experiments allows us to estimate the Ti

magnetic moment averaged over the total probing depth to be of the order of $10^{-2} \mu_B$ per atom (Supplementary Note 2). This value is in agreement with those obtained from the DFT calculations presented below as well as from neutron reflectometry on LAO/STO superlattices³² and recent X-ray magnetic circular dichroism experiments on similarly prepared LAO/STO-conducting interfaces³³.

First-principles calculations. To elucidate the origin of the observed onset of conductivity below 4 uc of LAO, DFT calculations were performed on Co(*m*)/LAO(*n*)/STO(001) (see Fig. 4) with the all-electron full-potential linearized augmented plane wave, as implemented in the WIEN2k code^{34,35}. For the exchange-correlation functional, we used the generalized gradient approximation (GGA)³⁶. The influence of electronic correlations beyond GGA is discussed in the Supplementary Note 3 (see also Supplementary Fig. 4). The in-plane lattice parameter is set to the GGA equilibrium lattice constant of STO ($a_{\text{STO}} = 3.92 \text{ \AA}$) and the atomic positions are fully relaxed within tetragonal symmetry. More details are provided in ref. 18 (see also the Methods section and Supplementary Note 3). Figure 4a shows the layer-resolved density of states of a (001)-oriented STO substrate (4.5-uc thick) covered with one monolayer (ML) of Co. In contrast to the uncovered STO(001) substrate (not shown here), where the Fermi level is pinned at the top of the valence band defined by surface states at the topmost TiO₂ layer, for Co/STO(001) the Fermi energy E_F shifts to the bottom of the Ti conduction band, leaving the Ti 3*d* band empty.

A similar change is observed when capping LAO/STO(001) with Co: In the uncovered LAO(1 uc)/STO system, the Fermi level lies at the top of the valence band (see Fig. 4b), determined by O 2*p* states of the surface AlO₂ layer, while the conduction band minimum is 2 eV above the Fermi energy and is determined by Ti 3*d* states. Adding a Co capping layer shifts the Fermi level to the bottom of the conduction band in Co/LAO(1 uc)/STO (see Fig. 4c). In contrast to LAO(1 uc)/STO and Co/STO, in Co/LAO(1 uc)/STO the Ti 3*d* band is now partially occupied, with a small spin polarization of -0.02 to $-0.03 \mu_B$ per Ti. Hence a metallic bilayer is formed in Co/LAO/STO, with a conducting surface (Co) and a conducting buried interface (STO side), consistent with the transport data. Furthermore, the Ti 3*d* band occupation increases weakly with LAO thickness (see Supplementary Figs 5 and 6). Adding the Co capping layer

(largely) cancels the internal potential buildup within the polar LAO film. As found previously¹⁸, the position of the Fermi level with respect to the conduction band minimum in STO is determined by the work function of the metallic contact (4.72 eV for 1 ML Co and 4.28 eV for 3 ML Co). This, together with the still persisting polar discontinuity at the LAO/STO interface leads to a finite occupation of the Ti 3*d* band at the interface.

Next, we explore the preferential orbital occupancy of the electronic system. The electron density of Co/LAO(1 uc)/STO, integrated between $E_F - 0.50 \text{ eV}$ and E_F reveals predominant d_{xy} orbital polarization of Ti in the interface layer and d_{xz}/d_{yz} character in deeper layers (see Fig. 4d), which can also be seen on the projected density of states in Fig. 4e. The orbital polarization is consistent with the structural distortions of the octahedra within the Co/LAO(1 uc)/STO heterostructure: We find that the average distance between the apical oxygens on both sides of Ti in the [001] direction is 3.92 Å for the interfacial (IF) and 3.99 Å for the IF-1 layers, respectively. In line with the experimentally determined t_{2g} splittings (Fig. 3d–f), we find that a shortened (expanded) TiO₆ octahedra average size in the [001] direction corresponds to d_{xy} orbitals lying lower (higher) in energy.

Discussion

Using four-point transport experiments, we have revealed the presence of metallic conduction at the LaAlO₃/SrTiO₃ interface for Co/LaAlO₃(*n*)/SrTiO₃ heterostructures with LaAlO₃ thicknesses $1 \text{ uc} \leq n \leq 4 \text{ uc}$. The linear dichroism observed through XAS evidences a compressive tetragonal distortion of the TiO₆ octahedra for cobalt-capped and uncapped LaAlO₃/SrTiO₃ systems. Making use of atomic multiplet calculations, we found that in Co/LaAlO₃/SrTiO₃ the Ti orbitals reconstruct from the situation in bare SrTiO₃ substrates. As a result, the lowest energy level has a d_{xy} orbital character for Co/LaAlO₃/SrTiO₃ systems, compared with d_{xz}/d_{yz} for the bare SrTiO₃. DFT calculations support this picture and predict structural distortions that agree with those inferred from XAS. Further, they indicate a finite occupancy of the Ti 3*d* bands at the Fermi energy for the Co/LaAlO₃(1 uc)/SrTiO₃ heterostructure, with a predominant d_{xy} orbital character within the interfacial TiO₂ layer. The metallic Co overlayer thus appears to modify the electrostatic boundary conditions of the LAO/STO system, leading to the occupation of the Ti 3*d* bands. These observations support the electrostatic origin of the quasi-two-dimensional electronic systems at the

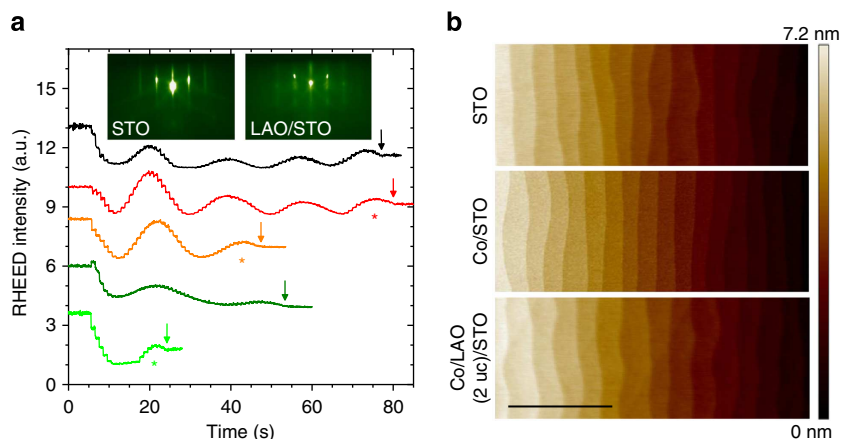


Figure 5 | In situ RHEED and ex situ AFM characterizations. (a) Monitoring of the RHEED (01) diffraction peak intensity versus time during the epitaxial growth of LAO films of various thicknesses (1–4 uc) on STO substrates. Inset: typical RHEED pattern of (left) an STO substrate, and (right) a 4-uc LAO thin film on STO, taken at 730°C in an oxygen partial pressure of 2.0×10^{-4} mbar. Arrows indicate the end of the growth. Asterisks designate samples later covered with a Co/AlO_x capping. (b) AFM topography of a TiO₂-terminated STO substrate and of Co/STO and Co/LAO(2 uc)/STO samples. The 2-nm Co thin film reproduces the steps and terraces of the terminated substrate. Scale bar, 1 μm.

LAO/STO interface as proposed in the polar catastrophe model^{17,37}, which suggests that cationic intermixing across the interface³⁸ or oxygen vacancies^{39–41} only play a marginal role.

For spintronics and tunnelling spectroscopy applications, it is necessary to control the tunnel barrier resistance, which is usually achieved by tuning its thickness. In the LaAlO₃/SrTiO₃ case, a stringent limitation for efficient tunnelling was the existence of a minimum thickness of 4 uc of LaAlO₃ for the onset of conductivity. Our findings should therefore considerably facilitate spin injection^{42,43} or tunnel spectroscopy studies^{44–46} only achievable in perpendicular geometries, thereby paving the way toward LaAlO₃/SrTiO₃-based electronic and spintronic tunnelling devices with tunable tunnel resistances.

Methods

Samples fabrication. The LaAlO₃ (LAO) films were grown by PLD on 5 × 5 mm TiO₂-terminated (001)-oriented SrTiO₃ (STO) substrates. A single-crystal LAO target was ablated by a KrF (248 nm) excimer laser at a repetition rate of 1 Hz and with a fluence of ~1 J cm⁻². The LAO deposition was performed in an oxygen partial pressure of 2.0 × 10⁻⁴ mbar and at a substrate temperature of 730 °C. Substrate-to-target distance was 63 mm. The layer-by-layer growth mode allowed us to precisely control the LAO thickness through real-time monitoring of reflection high-energy electron diffraction intensity oscillations (see Fig. 5a). The samples were then annealed for 30 min in about 400 mbar of oxygen at 500 °C (refs 39,40). Finally, the LAO/STO heterostructures were cooled at 25 °C min⁻¹ and kept in the same oxygen pressure for ~30 to 60 min. PLD growth was followed by *in situ* deposition of a metallic cobalt electrode by magnetron sputtering at room temperature in a pure Ar atmosphere of 4.5 × 10⁻⁴ mbar, resulting in a clean Co/LAO interface. The 2–2.5-nm Co thin films were capped with a 3-nm AlO_x layer to prevent cobalt oxidation. For the Co/STO sample, the same procedure of thermal and pressure cycles as the one described above were applied to the TiO₂-terminated STO substrate, skipping only the LAO deposition step, before the Co deposition.

AFM characterization. We performed an atomic force microscopy (AFM) topography study of uncapped 2-nm Co films grown on a TiO₂-terminated STO substrate and on an LAO/STO sample (see Fig. 5b). The Co was left to oxidize in air, which we believe could only increase surface roughness compared with Co metallic films capped with AlO_x. We estimate the root mean square surface roughness value (R_q) of the Co film by averaging over four 3 × 3 μm² images from different locations across the sample. $R_q = 1.49$ Å and 1.33 Å for Co films grown on the STO substrate and the LAO(2 uc)/STO, respectively. For comparison, the surface roughness of a terminated STO substrate from the same batch is of 1.50 Å. The surface roughness values are in fact dominated by the vicinal atomic steps and terraces of the substrate: considering 3.9 Å steps height leads to $R_q = 1.13$ Å. The AFM characterization study supports the smoothness and continuity of the 2-nm Co layer and suggests full coverage of the STO or LAO surfaces by the Co thin films.

DFT calculations. DFT calculations were performed using the all-electron full-potential linearized augmented plane wave method, as implemented in the WIEN2k code^{34,35}. For the exchange-correlation potential, we used the GGA³⁶. The muffin-tin spheres of the atoms were taken as: 2.3, 1.8 and 1.6 a.u. for La/Sr, Ti/Co/Al and O, respectively. The energy cutoff for the plane wave representation in the interstitial is $E_{\text{max}}^{\text{wf}} = 19$ Ry for the wave functions. The spherical harmonics inside the muffin-tin spheres are expanded up to $l_{\text{max}} = 10$, while the plane wave expansion of the charge density was truncated at $G_{\text{max}} = 12$ a.u.⁻¹, where a.u. stands for atomic units. The integrals over the Brillouin zone are performed with 36 k -points in the irreducible part of the Brillouin zone using the Monkhorst-Pack special k -points approach⁴⁷. We have chosen a symmetric slab with LAO and Co layers on both sides of the 4.5-uc-thick STO substrate and a vacuum region between the slab and its periodic images of at least 10 Å. The Co atoms are adsorbed on top of the oxygen ions at the surface of TiO₂ or AlO₂. The in-plane lattice parameter is set to the GGA equilibrium lattice constant of STO ($a_{\text{STO}} = 3.92$ Å), and the atomic positions are fully relaxed within tetragonal symmetry.

References

- Hwang, H. Y. *et al.* Emergent phenomena at oxide interfaces. *Nat. Mater.* **11**, 103–113 (2012).
- Ohtomo, A. & Hwang, H. Y. A high-mobility electron gas at the LaAlO₃/SrTiO₃ heterointerface. *Nature* **427**, 423–426 (2004).
- Thiel, S., Hammerl, G., Schmehl, A., Schneider, C. W. & Mannhart, J. Tunable quasi-two-dimensional electron gases in oxide heterostructures. *Science* **313**, 1942–1945 (2006).
- Ben Shalom, M., Sachs, M., Rakhmilevitch, D., Palevski, A. & Dagan, Y. Tuning spin-orbit coupling and superconductivity at the SrTiO₃/LaAlO₃ interface: a magnetotransport study. *Phys. Rev. Lett.* **104**, 126802 (2010).
- Caviglia, A. D. *et al.* Tunable Rashba spin-orbit interaction at oxide interfaces. *Phys. Rev. Lett.* **104**, 126803 (2010).
- Reyren, N. *et al.* Superconducting interfaces between insulating oxides. *Science* **317**, 1196–1199 (2007).
- Caviglia, A. D. *et al.* Electric field control of the LaAlO₃/SrTiO₃ interface ground state. *Nature* **456**, 624–627 (2008).
- Bell, C. *et al.* Dominant mobility modulation by the electric field effect at the LaAlO₃/SrTiO₃ interface. *Phys. Rev. Lett.* **103**, 226802 (2009).
- Brinkman, A. *et al.* Magnetic effects at the interface between non-magnetic oxides. *Nat. Mater.* **6**, 493–496 (2007).
- Ariando, Wang, X. *et al.* Electronic phase separation at the LaAlO₃/SrTiO₃ interface. *Nat. Commun.* **2**, 188 (2011).
- Bert, J. A. *et al.* Direct imaging of the coexistence of ferromagnetism and superconductivity at the LaAlO₃/SrTiO₃ interface. *Nat. Phys.* **7**, 767–771 (2011).
- Dikin, D. A. *et al.* Coexistence of superconductivity and ferromagnetism in two dimensions. *Phys. Rev. Lett.* **107**, 056802 (2011).
- Li, L., Richter, C., Mannhart, J. & Ashoori, R. C. Coexistence of magnetic order and two-dimensional superconductivity at LaAlO₃/SrTiO₃ interfaces. *Nat. Phys.* **7**, 762–766 (2011).
- Cen, C., Thiel, S., Mannhart, J. & Levy, J. Oxide nanoelectronics on demand. *Science* **323**, 1026–1030 (2009).
- Li, L. *et al.* Very large capacitance enhancement in a two-dimensional electron system. *Science* **332**, 825–828 (2011).
- Förg, B., Richter, C. & Mannhart, J. Field-effect devices utilizing LaAlO₃-SrTiO₃ interfaces. *Appl. Phys. Lett.* **100**, 053506 (2012).
- Nakagawa, N., Hwang, H. Y. & Muller, D. A. Why some interfaces cannot be sharp. *Nat. Mater.* **5**, 204–209 (2006).
- Arras, R., Ruiz, V. G., Pickett, W. E. & Pentcheva, R. Tuning the two-dimensional electron gas at the LaAlO₃/SrTiO₃(001) interface by metallic contacts. *Phys. Rev. B* **85**, 125404 (2012).
- van der Pauw, L. A method of measuring the resistivity and Hall coefficient on lamellae of arbitrary shape. *Philips Tech. Rev.* **20**, 220–224 (1958).
- Popović, Z., Satpathy, S. & Martin, R. Origin of the two-dimensional electron gas carrier density at the LaAlO₃ on SrTiO₃ interface. *Phys. Rev. Lett.* **101**, 256801 (2008).
- Pentcheva, R. *et al.* Parallel electron-hole bilayer conductivity from electronic interface reconstruction. *Phys. Rev. Lett.* **104**, 166804 (2010).
- Joshua, A., Pecker, S., Ruhman, J., Altman, E. & Ilani, S. A universal critical density underlying the physics of electrons at the LaAlO₃/SrTiO₃ interface. *Nat. Commun.* **3**, 1129 (2012).
- Caviglia, A. D. *et al.* Two-dimensional quantum oscillations of the conductance at LaAlO₃/SrTiO₃ interfaces. *Phys. Rev. Lett.* **105**, 236802 (2010).
- Ben Shalom, M., Ron, A., Palevski, A. & Dagan, Y. Shubnikov-De Haas oscillations in SrTiO₃/LaAlO₃ interface. *Phys. Rev. Lett.* **105**, 206401 (2010).
- Ohresser, P. *et al.* DEIMOS: a beamline dedicated to dichroism measurements in the 350–2500 eV energy range. *Rev. Sci. Instrum.* **85**, 013106 (2014).
- Cowan, R. D. *The Theory of Atomic Structure and Spectra* (University of California Press, 1981).
- de Groot, F. M. F., Fuggle, J., Thole, B. & Sawatzky, G. L_{2,3} x-ray-absorption edges of d0 compounds: K⁺, Ca²⁺, Sc³⁺, and Ti⁴⁺ in O_h (octahedral) symmetry. *Phys. Rev. B* **41**, 928–937 (1990).
- Mattheiss, L. Energy bands for KNiF₃, SrTiO₃, KMoO₃, and KTaO₃. *Phys. Rev. B* **6**, 4718–4740 (1972).
- Stavitski, E. & de Groot, F. M. F. The CTM4XAS program for EELS and XAS spectral shape analysis of transition metal L edges. *Micron* **41**, 687 (2010).
- Salluzzo, M. *et al.* Structural and electronic reconstructions at the LaAlO₃/SrTiO₃ interface. *Adv. Mater.* **25**, 2333–2338 (2013).
- Salluzzo, M. *et al.* Orbital reconstruction and the two-dimensional electron gas at the LaAlO₃/SrTiO₃ interface. *Phys. Rev. Lett.* **102**, 166804 (2009).
- Fitzsimmons, M. *et al.* Upper limit to magnetism in LaAlO₃/SrTiO₃ heterostructures. *Phys. Rev. Lett.* **107**, 217201 (2011).
- Salluzzo, M. *et al.* Origin of interface magnetism in BiMnO₃/SrTiO₃ and LaAlO₃/SrTiO₃ heterostructures. *Phys. Rev. Lett.* **111**, 087204 (2013).
- Schwarz, K. & Blaha, P. Solid state calculations using wien2k. *Comput. Mater. Sci.* **28**, 259–273 (2003).
- Blaha, P., Schwarz, K., Madsen, G. K. H., Kvasnicka, D. & Luitz, J. WIEN2k, An Augmented Plane Wave Plus Local Orbitals Program for Calculating Crystal Properties (Vienna University of Technology, 2001).
- Perdew, J. P., Burke, K. & Ernzerhof, M. Generalized gradient approximation made simple. *Phys. Rev. Lett.* **77**, 3865–3868 (1996).
- Reinle-Schmitt, M. L. *et al.* Tunable conductivity threshold at polar oxide interfaces. *Nat. Commun.* **3**, 932 (2012).

38. Willmott, P. *et al.* Structural basis for the conducting interface between LaAlO₃ and SrTiO₃. *Phys. Rev. Lett.* **99**, 155502 (2007).
39. Cancellieri, C. *et al.* Influence of the growth conditions on the LaAlO₃/SrTiO₃ interface electronic properties. *EPL (Europhys. Lett.)* **91**, 17004 (2010).
40. Basletic, M. *et al.* Mapping the spatial distribution of charge carriers in LaAlO₃/SrTiO₃ heterostructures. *Nat. Mater.* **7**, 621–625 (2008).
41. Liu, Z. Q. *et al.* Origin of the two-dimensional electron gas at LaAlO₃/SrTiO₃ interfaces: the role of oxygen vacancies and electronic reconstruction. *Phys. Rev. X* **3**, 021010 (2013).
42. Fert, A. & Jaffrès, H. Conditions for efficient spin injection from a ferromagnetic metal into a semiconductor. *Phys. Rev. B* **64**, 184420 (2001).
43. Reyren, N. *et al.* Gate-controlled spin injection at LaAlO₃/SrTiO₃ interfaces. *Phys. Rev. Lett.* **108**, 186802 (2012).
44. Breitschaft, M. *et al.* Two-dimensional electron liquid state at LaAlO₃/SrTiO₃ interfaces. *Phys. Rev. B* **81**, 153414 (2010).
45. Ristic, Z. *et al.* Photodoping and in-gap interface states across the metal-insulator transition in LaAlO₃/SrTiO₃ heterostructures. *Phys. Rev. B* **86**, 045127 (2012).
46. Richter, C. *et al.* Interface superconductor with gap behaviour like a high-temperature superconductor. *Nature* **502**, 528–531 (2013).
47. Monkhorst, H. J. & Pack, J. D. Special points for brillouin-zone integrations. *Phys. Rev. B* **13**, 5188–5192 (1976).

Acknowledgements

We acknowledge fruitful discussions with C. Deranlot. We would like to thank E. Jacquet for his support with the PLD and sputtering systems. We thank D. Sando and L. Phillips

for a careful reading of the manuscript. We acknowledge SOLEIL for provision of synchrotron radiation facilities (project no. 20111079). This work was partly supported by the European Research Council (ERC Advanced Grant FEMMES, No. 267579), the German Science Foundation through project C3 within SFB/TR80 and grant h0721 for computational time at the supercomputers of the Leibniz Rechenzentrum, Garching.

Author contributions

A.B. and M.B. supervised the project. E.L. and N.R. fabricated the samples, performed and analysed the transport measurements. E.L., N.R., R.M., V.C., F.C., P.O. and A.B. performed synchrotron measurements. E.L., N.R., R.M. and P.O. analysed the synchrotron data. D.D. and R.P. performed the *ab-initio* calculations. All authors contributed to interpretation of the results. E.L., N.R., D.D. and R.P. wrote the manuscript with inputs from P.O. and M.B.

Additional information

Supplementary Information accompanies this paper at <http://www.nature.com/naturecommunications>

Competing financial interests: The authors declare no competing financial interests.

Reprints and permission information is available online at <http://npg.nature.com/reprintsandpermissions/>

How to cite this article: Lesne, E. *et al.* Suppression of the critical thickness threshold for conductivity at the LaAlO₃/SrTiO₃ interface. *Nat. Commun.* **5**:4291 doi: 10.1038/ncomms5291 (2014).